Mineral-Hydrogel Composites for Mitigating Harmful Algal Bloom and Supplying Phosphorous for Photo-biorefineries

Zhengyang Xiao[§], Albern X. Tan[§], Vincent Xu, Young-Shin Jun,* and Yinjie J. Tang*

Department of Energy, Environmental and Chemical Engineering, Washington University, St. Louis, MO, 63130, U.S.A.

[§]: Equal contributions

*corresponding authors:

YSJ (ORCID: 0000-0003-4648-2984): ysjun@seas.wustl.edu

YJT (ORCID: 0000-0002-5112-0649): yinjie.tang@wustl.edu

Abstract

Harmful algal blooms (HAB) are a major environmental concern in eutrophic aquatic systems. To mitigate HABs and recover the phosphorus that drives algal growth, this study developed hydrogel composites seeded with calcium phosphate and wollastonite particles, which first adsorb phosphate (P) and then precipitate it as calcium phosphate. Using a fast-growing cyanobacterium, *Synechococcus elongatus* 2973, as a model microalga, we found that the mineral-hydrogel composites reduced dissolved P in BG11 media from 5.1 mg/L to 0.31 mg/L, initially reducing the biomass growth rate by up to 73% and ultimately reducing the total biomass concentration by 75%. When applied to municipal wastewater and agricultural run-off, the composites removed 96% and 91% of the dissolved P, respectively. Moreover, when the recovered P-enriched composites were reused as a slow-release bio-compatible fertilizer in a photobioreactor, they effectively supported algal growth without blocking light and interfering with photosynthesis. The P-enriched composites could tune the P concentration in the culture medium and significantly promote algal lipid accumulation. This study demonstrates the mineral-hydrogel composites' potential to treat point sources of P pollution and subsequently facilitate photoautotrophic biofuel production as a substrate, effectively recycling the captured P.

Keywords: *cyanobacteria*, hydrogels, photo-biorefinery, shading effect, biofuel

Introduction

The large release of phosphorus (P)-rich wastewater into environments (Correll, 1998) and P from agricultural run-off (Daniel et al., 1998; Trottet et al., 2021) leads to excessive algal growth in aquatic environments (Davis et al., 2015). Since 1940, P fertilizer consumption in the United States has increased by over 18-fold (Jasinski, 2020). Worldwide, increased P in water resources has caused and worsened harmful algal blooms (HABs) (Gobler, 2020). HABs deteriorate surface water quality, affecting aquatic life and increasing water treatment costs, threatening environmental and economic sustainability (O'Neill et al., 2018). In HABs, cyanobacteria are prominent algal species (Bullerjahn et al., 2016), which not only generate cyanotoxins (Paerl et al., 2001), but also fix atmospheric nitrogen to elevate algal growth (Berman-Frank et al., 2003; Zehr, 2011). Compounding the problem related to P resource management, P is sourced mainly from non-renewable mined phosphorus rock (Wurtsbaugh et al., 2019). Thus, its recovery from wastewater and agricultural run-off is critically important for sustainable P management (Carpenter and Bennett, 2011; Mayer et al., 2016; Reijnders, 2014).

Reducing P concentrations in water systems is an effective HAB controlling strategy (Yaakob et al., 2021). Hence, multiple effective P removal and recovery methods have been developed. For example, biological P removal through sludge separation is a common technique for municipal wastewater treatment. Struvite precipitation, a well-established P recovery method, targets wastewater streams with high P concentrations (Kumar and Pal, 2015). Adsorption of P using sorbents, such as ion exchange materials (Guida et al., 2021; Zarrabi et al., 2014), metal oxides (Li et al., 2016), biochars (Bolton et al., 2019; Yao et al., 2013), and activated carbon (Braun et al., 2019; Mahardika et al., 2018; Wang et al.,

2018), have also been suggested for removing P from wastewater and then reusing it as fertilizer (Bacelo et al., 2020; Kumar et al., 2019a). However, current P removal technologies still have three innate limitations. First, most adsorbents are applied as micrometer-scale powder-like materials that are difficult to separate from water after their use. If applied in fixed bed media reactors, they require sufficient hydraulic residence time to remove P and extra pumping energy to overcome the pressure drop across the packed media. Second, engineering an adsorbent with a high P affinity at low P concentrations is still challenging. For example, non-specific electrostatic adsorption sites have a low affinity for phosphate, especially in the presence of competing anions (Kumar et al., 2019a). Methods relying on inner-sphere complexation, ion exchange, or layered metal hydroxides (Bacelo et al., 2020; dos Santos et al., 2021; Kumar et al., 2019a; Wu et al., 2020; Zhang et al., 2020; Zhi et al., 2020), can achieve high selectivity and high phosphate affinity. However, their high phosphate binding strength necessitates costly regeneration techniques using harsh chemicals, creating a tradeoff between P selectivity and recovery costs. Third, P removal from wastewater is expensive, with an average cost of $52 per pound of P removed (Bashar et al., 2018), and the cost of achieving ultra-low concentrations (< 0.15 mg-P/L) can be higher (Kumar et al., 2019a). Furthermore, rather than discarding the absorbent as solid waste, reusing it in different commercial processes (upcycling) can offset the cost of P removal (Shepherd et al., 2016).

To address these limitations, recently we developed mineral-hydrogel composites that immobilized *in situ* formed calcium phosphate (CaP) mineral seeds in millimeter-scale hydrogel composite beads (Kim et al., 2018; Tan et al., 2021b). These millimeter-sized particles are easy to separate from water. The mineral seeds within the composites decreased the CaP nucleation barrier and facilitated heterogeneous

nucleation and growth of CaP (Kim et al., 2018). In this way, the novel composites leverage CaP mineral precipitation chemistry, enabling a high P-loading (removal) of 96.4 mg P g^{-1} dry seed at a low P concentration of 0.7 mg-P/L (Kim et al., 2018). These composites were further improved by incorporating calcium silicate hydrate (CSH) minerals to raise the composites' internal pH and provide additional calcium for CaP formation (Tan et al., 2021a). Compared to the mineral-hydrogel composite formulation of Kim et al. (2018), the CaP + CSH/Ca-Alg composite offered several advantages. Its phosphate-removal kinetics were twice as fast as those of CaP-only mineral-hydrogel composites, it had lower chemical requirements for synthesis (e.g., 75% less calcium and ~70% less phosphate), and it even captured phosphorus from hydroxyapatite-undersaturated solutions (Tan et al., 2021a). The results showed that calcium silicate mineral dissolution synergistically works with the CaP mineral seeds during phosphate removal. To advance further, for the current study, we designed new mineral-hydrogel composites with CaP and wollastonite ($CaSiO_3$). Wollastonite, a naturally occurring calcium silicate mineral, has lower solubility (Chen et al., 2004; Jambor et al., 2002) than the previously used CSH mineral seeds. Wollastonite also has slower dissolution kinetics (~$10^{-13.5}$ mol/m^2s at pH ~10 for wollastonite) (Schott et al., 2012) than CSH ($10^{-10.4}$ – $10^{-12.4}$ mol/m^2s at pH ~ 10) (Trapote-Barreira et al., 2014), leading to a more controlled P capture within the composites and avoiding the formation of potentially mobile CaP mineral precipitates in solution which can be induced by fast CSH dissolution. (Tan et al., 2021b).

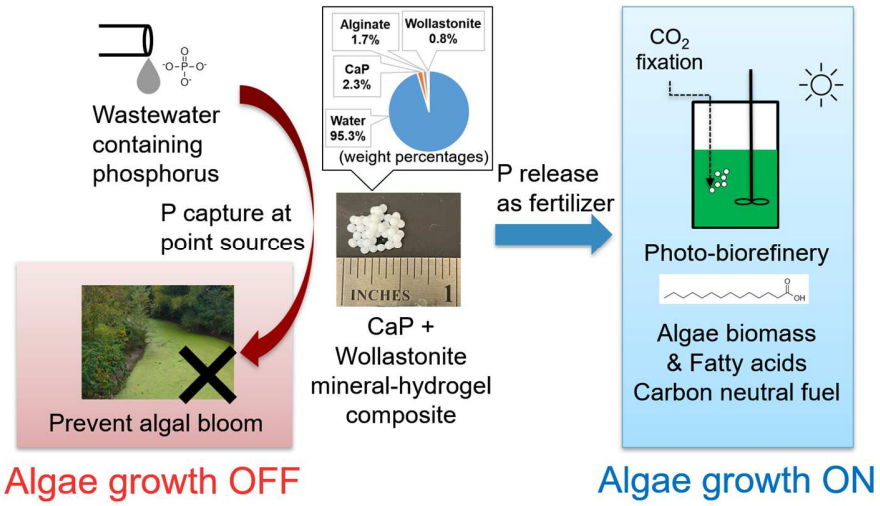

Fig. 1: P management framework of the novel CaP + wollastonite mineral-hydrogel composite.

After we developed the new CaP + wollastonite mineral-hydrogel composites, for a better circular P utilization, we explored its use in promoting algal growth in photobioreactors. While algae can cause environmental hazards, they produce valuable food, chemicals, and biofuels from only light and CO_2 (Li et al., 2019; Yu et al., 2013). Algal species have a luxury P-uptake, and thus algal refineries consume significant P (Solovchenko et al., 2019a; Solovchenko et al., 2019b). In the past, diverse absorbents, such as activated carbon (Braun et al., 2019; Li et al., 2018) and biochars (Bolton et al., 2019; Dalahmeh et al., 2020), were used for P capture from wastewater and then reused as P sources. However, these absorbents are not directly usable in photo-biorefineries because their dark, fine particles absorb light. In contrast, mineral-hydrogel composites are a promising P-resource for algae cultivation, releasing P with minimal light interference. Thus, utilizing our newly developed mineral-hydrogel composites, this study examines whether the composites can control HAB by removing P from eutrophic sources and can resupply P for photobioreactor cultivation. Specifically, we investigated three aspects of their application: (1) the

105 composites' P capture/release kinetics and interactions with cyanobacteria when applied directly or as a
106 pretreatment, (2) the growth responses of a fast-growing cyanobacterial species and a natural algal
107 community after P capture, and (3) the composite's potential for treating municipal wastewater and
108 agricultural run-off. Overall, distinct from our previous studies (Kim et al., 2018; Tan et al., 2021b), here
109 we focus on the interactions of our newly developed mineral-hydrogel composites with a model
110 cyanobacterium, and we evaluate their potential as a P-supply for photobioreactors. To assess their
111 broader application potential, the mineral-hydrogel composites in this study were also tested in more
112 complex aqueous environments than in our previous studies (e.g., BG11 medium or complex wastewater
113 samples). Ideally, the developed composites will assist us to enable efficient P capture and release,
114 alleviate HAB's adverse impacts, and facilitate sustainable bioproduction (**Fig. 1**).

115 ## Materials and methods

116 **Synthesis of mineral-hydrogel composites.** A precursor solution was prepared using 0.6% w/w sodium
117 alginate with 40 mM of Na_2HPO_4 and 2.6 g/L of wollastonite (NYAD 5000®, obtained from NYCO, 803
118 Mountain View Drive, Willsboro, NY)). The wollastonite had a median particle size of 3 μm. In
119 preliminary tests, we found that mineral-hydrogel composites containing CaP alone, as in our previous
120 work (Kim et al., 2018), were unstable in photo-bioreactor environments, because the reactor can be
121 undersaturated with respect to hydroxyapatite (HA) (**Figure S4**). Therefore, to improve the composite
122 performance under HA undersaturated conditions, we added wollastonite, which can supply calcium from
123 the hydrogel matrix for alginate crosslinking and mechanical stability. We then verified that adding 2.6
124 g/L of wollastonite to the composite formulation provided increased mechanical stability in photo-

bioreactor environments (**Figure S4**) and confirmed the mineral-hydrogel composite's P-removal ability. Subsequently, to focus on the response of the algal system to composites, we maintained the same mineral-hydrogel composite formulation throughout all the experiments.

To synthesize mineral-hydrogel composites, the precursor solution was well-mixed and then dripped into a gelation solution containing 100 mM $CaCl_2$ and 20 mM NaOH (pH = 12) using a syringe (HenkeSassWolf, Tuttlingen, Germany) with a 0.514 mm internal diameter needle (Becton, Dickenson and Company, Franklin Lakes, NH, USA). A syringe pump (KD scientific, MA, USA) was set to deliver 4 mL/minute, and the needle outlet was positioned 5 cm above the gelation solution. The volume ratio (precursor to gelation bath) was set at 1:10, based on our previous work (Kim et al., 2018; Tan et al., 2021a). After the hydrogel beads had formed and matured under stirring in the gelation solution for 4 hours, they were rinsed three times in DI (deionized) water (≥ 18.1 MΩ·cm, obtained using a NANOpure® Diamond™ system). The dry weight percentages of mineral-hydrogel composites were based on the dry weights of the precursor materials: 36% alginate, 48% CaP mineral seed, and 16% wollastonite. To determine the water content in the wet composite beads, we measured the weight difference before and after drying them on a heating plate (n = 2). The water content of the composites was 95.3 ± 0.1% w/w. Other components were 2.3% CaP, 1.7% alginate, and 0.8% wollastonite by weight.

P capture and release by mineral-hydrogel composites. The dose of composites into a P-rich solution was expressed in wet weight percentages, specifically 1%, 2%, and 5% (corresponding to 10 g/L, 20 g/L, and 50 g/L). Blue-green medium (BG11), used as a synthetic P-rich wastewater, was used for cyanobacterial growth (Abernathy et al., 2017). The initial pH of the BG11 was 7.5. To study P capture

and release, BG11 was mixed with mineral-hydrogel composites in a shaking flask and shaken at 100 rpm at room temperature for 24 hours. To capture P from realistic waste streams, we tested two complex water systems: First, 20 mL of municipal wastewater from the Missouri River Treatment Plant was mixed with 1 g of composites (5% w/w composite wet weight) in a flask, with a stir bar providing agitation. Second, we treated Bold 3N media (UTEX, Texas) with 5% composites. Note that Bold 3N is an undefined HAB medium containing soil water, vitamins, and tracer metals, which mimics agricultural run-off water. Then the treated water samples were diluted with P-free BG11 medium to simulate P release to a larger waterbody. After they had captured P from municipal wastewater, the P-recovered composites were used to release P to P-free BG11 over multiple cycles. In each cycle, P-free BG11 was mixed with 5% (50 g/L) P-recovered composites in a shaking flask at 100 rpm and room temperature for 24 hours.

For P concentration measurement, 0.2 mL samples were taken for ion chromatography (Thermo Scientific Dionex Integrion RFIC) analysis. An AS18 anion testing method was used: sample delivery speed =1.6 mL/min, delay volume = 70 µL, flush factor = 3, conductivity cell temperature = 35 °C, column heater = off, and total run time = 18 minutes/sample (Wang et al., 2020). All P capture experiments were done in duplicate, and the +/- standard deviation (SD) was calculated.

Scanning Electron Microscopy (SEM) and Energy Dispersive X-ray Spectroscopy (EDS) Characterization. Mineral-hydrogel composites were dehydrated, swollen in pure ethanol, and then ground with a pestle in a mortar. Afterward, the fragmented sample was air-dried at room temperature, forming a powder that was sputtered with 10 nm of gold coating (Leica EM ACE High Vacuum Sputter Coater) for imaging by a SEM equipped with a backscattering electron detector (ThermoFisher Quattro S

165 E-SEM, ThermoFisher, Waltham, MA). EDS measurements were also performed (Oxford Instruments
166 EDS detector), and ImageJ 1.8 was used to analyze hydrogel composites and the mineral seed sizes from
167 SEM-BSE images. At least 10 sites per sample of the powders were imaged. For the EDS data presented
168 in the SI, at least 10 sites were examined to determine the Ca/P ratios. For Ca/P ratio determination, the
169 small interference from wollastonite (indicated by Si atomic percentage) was subtracted from the total
170 calcium atomic percentage. Other characteristics of the powders, such as their pore size and pore volume,
171 were not measured, because the dry surface area does not reflect the hydrated state of the mineral-
172 hydrogel composites.
173 **Algal culture.** *Synechococcus elongatus* 2973, a fast-growing cyanobacterium, was the model microalgae
174 (Abernathy et al., 2017). For seed culture preparations, cells freshly grown in normal BG11 were
175 centrifuged, and the pellets were washed once (using 0.9% NaCl solution) then resuspended into P-free
176 BG11 before inoculation. This step avoided P carry-over in the inoculum. The growth experiments (15
177 mL cultures) were all started at the same cell optical density, an OD_{730} of 0.1, in shake flasks at 160 rpm.
178 To mimic algal growth responding to different environmental conditions, algal cultivations were
179 conducted under different light conditions (continuous light intensity of either 100 or 200 μE m^{-2} s^{-1}) and
180 temperatures (30 or 37 °C). Four sets of experiments were performed to explore potential applications of
181 mineral-hydrogel composites. The first set examined cyanobacterial growth with treated synthetic
182 wastewater. We varied composite doses, temperature, and the light condition and observed the *S.*
183 *elongatus* growth response. BG11 was the synthetic wastewater medium. The composite doses were 1%
184 and 2% w/w (10 g/L and 20 g/L, respectively). The + P control was the untreated BG11 medium. In the

second set of experiments, we studied natural algal community growth in treated synthetic wastewater. On August 15, 2021, algae were sampled from a pond in Forest Park, St. Louis, Missouri, United States, 38.643282° N, 90.272553° W). The sampled algae were grown separately in pretreated and untreated BG11 media. The composite dose was 2% w/w (20 g/L), and the +P control was the untreated BG11 medium. The third set of experiments evaluated cyanobacterial growth with either municipal wastewater or agricultural run-off. To mimic releasing P to a large waterbody, the treated and untreated wastewaters were diluted with P-free BG11 in v/v ratios of 10x, 30x, and 100x and then used for *S. elongatus* growth. Real municipal wastewater was used as sampled (composition in **Table S1**), and Bold 3N medium was a proxy for agricultural run-off water. The municipal wastewater cation content (Na^+, K^+, Mg^{2+}, Ca^{2+}) was measured using inductively coupled plasma optical emission spectroscopy (ICP-OES) after the sample was digested using 5% w/w Nitric acid and 5% H_2O_2 at 80 ºC for 4 hours. The municipal wastewater anion content was measured by ion chromatography using the same procedure described above. The composite dose was 5% w/w (50 g/L). In the fourth experimental set, we examined cyanobacterial growth and lipid production under controlled release of P from mineral-hydrogel composites. P-recovered composites and new composites were separately added to P-free BG11 as slow-release fertilizers to promote lipid accumulation in *S. elongatus*. The composite dose was 1% w/w (10 g/L).

During all cultivations, the algal growth was monitored by either dry cell weights or OD_{730} using a UV-Vis spectrometer (Agilent Cary 60 UV-vis, CA). For each experiment, at least two replicates were performed. Cell morphologies were imaged by a microscope (Zeiss Axio Observer Z1, Germany).

Fatty acid quantification. Because algal fatty acids can be used as biodiesel fuels (Yu et al., 2013), we

examined *S. elongatus* fatty acid accumulation using P-recovered composites as fertilizer. The fatty acids methyl ester measurement followed the procedure in Amara et al. (Amara et al., 2016). Each time, 5 mL of cell culture was sampled, and the cell pellets after centrifugation were resuspended in 0.5 mL of 10% v/v H_2SO_4 in methanol, which contained 40 mg/L C19:0 fatty acid as an internal standard. Then 0.5 mL of chloroform was added. The mixture was transferred to a sealed glass vial and heated at 100 °C for one hour. The lysed cells were rapidly cooled by submerging them in cold water, and 1 mL of DI water was then added. The cell extracts were centrifuged, and the bottom chloroform layer was taken out and analyzed by a GC-MS (Agilent 7820A with HP-5m column and 5977E MSD). A standard curve was constructed by using a fatty acid methyl ester (FAME) standard solution (Millipore Sigma, St. Louis, USA). Three replicates were performed for each condition.

Statistics. Kinetic data curve fitting was done by using the MATLAB nlinfit function, which returned the 95% confidence interval and root-mean-square-error (rmse) of each parameter. A one-tail, two-sample Student's *t*-test was performed using the MATLAB ttest2 function.

Results and Discussion

Characterization of mineral-hydrogel composites and their P capture kinetics. The composites were imaged using SEM-EDS, both before and after 24 hours of P-removal reaction in cell-free BG-11. The representative images in **Fig. 2** clearly show micrometer-scale wollastonite mineral seeds (identified using EDS) and nanoscale CaP mineral seeds. Both before and after the reaction, CaP mineral seeds had two co-existing morphologies: (1) small, rounded, amorphous particles and (2) larger rod-shaped

224 particles. A sample of 32 amorphous particles seen in **Fig. 2a-I** had an average diameter of 94 nm ± 42
225 nm; a similar sample of 32 particles from **Fig. 2b-iii** had an average diameter of 130 nm ± 37 nm. A
226 sample of 32 particles from **Fig. 2a-ii** had an average length of 323 nm ± 75 nm and a width of 93 ± 20
227 nm. A similar sample from **Fig. 2b-iv** had an average length = 303 nm ± 62 nm, and a width of 90 ± 17
228 nm. Before the P-removal, distinct regions of amorphous and the elongated rod-shaped particles were
229 observed. However, after P-removal, while both particle morphologies were present, the shapes were less
230 clearly distinct. The heterogeneous nucleation and growth of CaP particles caused the more mixed particle
231 morphologies. Both before and after P removal, the Ca/P ratios, measured by EDS, did not differ between
232 the two CaP morphologies, with values ranging from 2.2–2.5 (**Fig. 2c, d** and **Fig. S2)**. In addition, based
233 on SEM-EDS elemental analysis, larger rectangular wollastonite particles, with lengths of ~2–5 μm, were
234 also visible (the scan areas are indicated by the purple boxes in **Fig. 2a, b**).

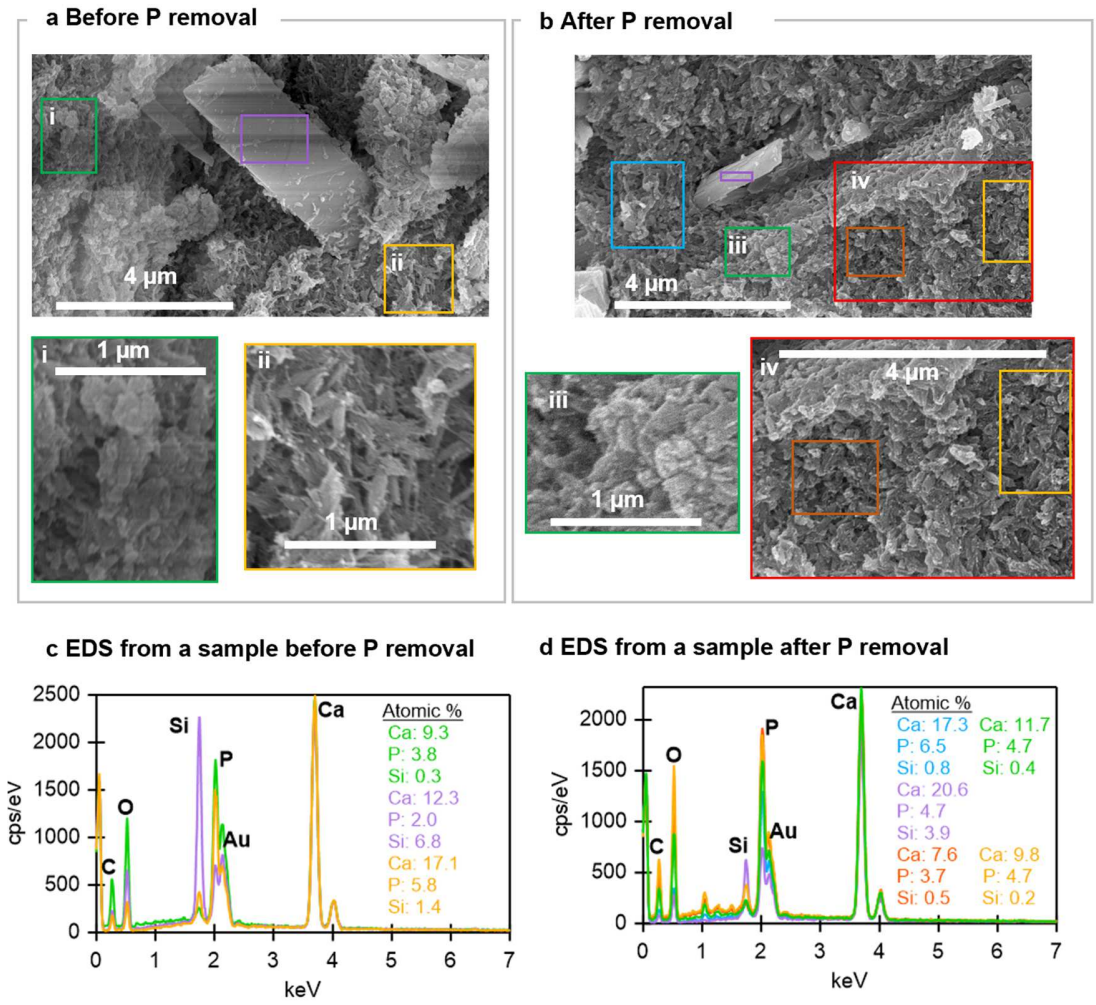

Fig. 2: SEM images of 40 mM CaP + 2.6 g/L wollastonite mineral-hydrogel composites and corresponding EDS scans: (a) Before P removal. The large rectangular wollastonite particle (purple box indicates EDS scan area) centered in the image is surrounded by two different morphology CaP particles (green and yellow boxes indicate EDS scan areas). (b) After P removal. The rectangular wollastonite particle (purple box indicates EDS scan area) in the image is surrounded by CaP particles (green, blue, yellow, and orange boxes indicate EDS scan areas). Both before and after P removal, more amorphous, rounded CaP particles (green and blue boxes) and more elongated rod-shaped CaP particles (shown in the yellow and red boxes) are observed, but their Ca/P ratios do not differ significantly (**Fig. S2)**. The colors of the lines in the EDS plots (c and d) indicate the results from the corresponding-colored boxes in the SEM images.

To test the removal of P by the synthesized mineral-hydrogel composites, we added them into BG11.

Fig. 3a, b, and **c** show that the composites effectively removed P from the BG11 medium. When 1%

composites (wet weight, 10 g-composites/L) were added to BG11 with an initial P concentration of 5.14 mg/l, they removed 83% of the P in 24 h (final P = 0.89 mg/L). When 2% composites were used, P removal was faster, with 92% P removed (final P = 0.43 mg/L). With 3% composites, the final P concentration was reduced by 94% (final P = 0.31 mg/L).

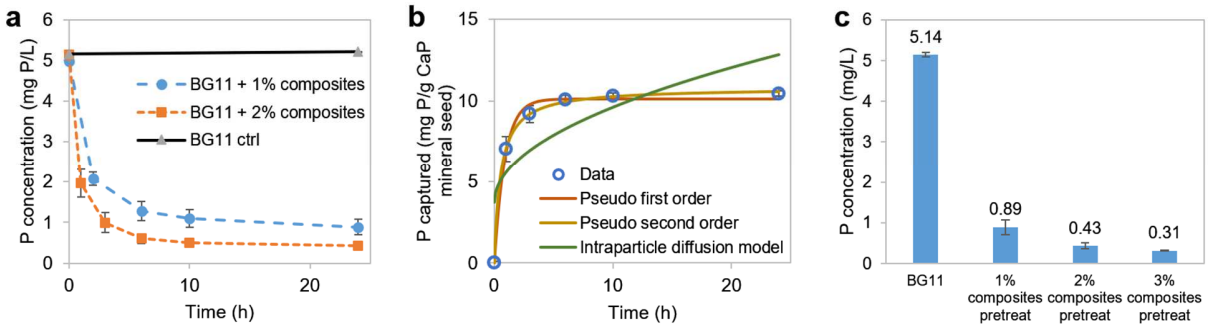

Fig. 3. (a) P removal kinetic data (n = 2). (b) The kinetic models used to describe the P capture process (n = 2). (c) Final P concentrations after composites pretreatment (n = 2). The experiments were at room temperature.

In the mineral-hydrogel composites, CaP mineral seeds and wollastonite are located close to each other. The CaP mineral seeds facilitate heterogeneous CaP nucleation and growth, while the wollastonite mineral seeds' dissolution locally increases the pH in the composites' microenvironment and provides calcium for CaP nucleation (Tan et al., 2021a). The seed particles formed inside the hydrogel composites reduce the nucleation energy barrier for new CaP formation from bulk water (Kim et al., 2018). The amorphous CaP growth follows Eq. 1 (Combes and Rey, 2010), and wollastonite participates in dissolution and ion exchange with the aqueous solution (Eq. 2 and 3) (Weissbart and Rimstidt, 2000; Xie and Walther, 1994).

$$9\,Ca^{2+} + x\,HPO_4^{2-} + (6-x)PO_4^{3-} + x\,OH^- \leftrightarrows Ca_9(PO_4)_{6-x}(HPO_4)_x(OH)_x \quad (1)$$

$$CaSiO_3 + 3H_2O \leftrightarrows Ca^{2+} + 2\,OH^- + H_4SiO_4 \quad (2)$$

$$\equiv (SiO)_2Ca + 2\,H^+ \leftrightarrows 2 \equiv SiOH + Ca^{2+} \quad (3)$$

During P transport from the bulk solution to the surface of composites, adsorption is the first step, followed by the heterogeneous nucleation and crystal growth of CaP. Therefore, adsorption isotherm models cannot fully describe such a dynamic process. Even so, it would be useful to provide a guideline to estimate P transport. Thus, we applied four reported kinetic models to simulate P transport (Cantor, 2003; Yao et al., 2013).

Table 1. Kinetic models and parameter estimation by regressions of the experimental data

Kinetic model	Assumption	Equation	Parameter 1	Parameter 2	rmse
Mass transfer *(Shuler and Kargi, 2002)*	P removal rate is linear to its aqueous concentration.	$\frac{d[P]}{dt} = -k_c([P] - [P]^*)$	k_c = 1.13±0.32 (h^{-1})	$[P]^*$ = 0.58±0.24 (mg/L)	0.16
First order *(Lin and Wang, 2009; Yao et al., 2013)*	P removal is a first order reaction with respect to available adsorption sites.	$\frac{dq_t}{dt} = K_1(q_e - q_t)$	K_1 = 1.13±0.32 (h^{-1})	q_e= 10.11±0.53 (mg/g)	0.36
Second order *(Lin and Wang, 2009; Yao et al., 2013)*	P removal is a second order reaction with respect to available adsorption sites.	$\frac{dq_t}{dt} = K_2(q_e - q_t)^2$	K_2 = 0.18±0.03 ($mg^{-1}g^1h^{-1}$)	q_e = 10.79±0.19 (mg/g)	0.094
Intraparticle diffusion *(Itodo et al., 2010)*	The bulk phase is well-mixed.	$q_t = K_i t^{\frac{1}{2}} + C$	K_i = 1.86±1.99 ($mg^1g^{-1}h^{-0.5}$)	C = 3.72±5.39 (mg/g)	2.76

±: 95% confidence interval, determined by MATLAB nlinfit.

In **Table 1**, the *mass transfer* model describes P removal from the aqueous solution. The *first order* and *second order* models assume the P capture processes are controlled by available adsorption sites and the P-loading (removal) equilibrium, q_e. The *intraparticle diffusion* model assumes intraparticle transport is rate-limiting ($\frac{1}{2}$ order dependence on time). The two parameters for each model were estimated based on experimental data, using MATLAB nlinfit. Among the four models, the *second order* model best fits

the experimental data (**Fig. 3b**), with the smallest root-mean-square-error (rmse) 0.094. Neither the *first order kinetics* nor the *intraparticle diffusion* model fits the experimental data well (Bujdák, 2020; Rudzinski and Plazinski, 2006), indicating that as we predicted, the P capture process is governed by multiple processes (diffusion, adsorption, precipitation, and heterogeneous CaP nucleation).

Treatment of synthetic wastewater using mineral-hydrogel composites to reduce algal growth. To evaluate the P removal efficacy of the composites for reducing HABs, we tested *S. elongatus* growth using two protocols: (1) direct introduction of the culture to the medium, and (2) pretreatment of the medium before inoculation. In the first protocol, the composites were mixed with *S. elongatus* cultures. **Fig. 4a-d** shows *S. elongatus* growth with composites under two different temperatures and two light intensities. Because the cyanobacterial P-uptake is highly efficient (Kromkamp et al., 1989; Ritchie et al., 2001), On average, the mixture of 1% composites with BG11 cultures showed only a moderate growth rate reduction over a 24 hour period, compared to the BG11 control (+ P ctrl) at each light and temperature condition, At 30°C, there was a 2% reduction (ns, n = 3) under 100 $\mu Em^{-2}s^{-1}$ (**Fig. 4a**), and a 14% reduction (ns, n = 3) under 200 $\mu Em^{-2}s^{-1}$ (**Fig. 4b**). At 37°C, there was a 16% reduction ($p < 0.01$, n = 3) under 100 $\mu Em^{-2}s^{-1}$ (**Fig. 4c**), and a 28% reduction ($p < 0.05$, n = 6) under 200 $\mu Em^{-2}s^{-1}$ (**Fig. 4d**).

In the second protocol, we pretreated the BG11 by adding the composites, and used the resulting P-reduced medium for algal growth. All the treated media showed significant reductions in cyanobacterial growth. For example, the cyanobacterial growth rate in the pretreated BG11 decreased by 73% ($p < 0.005$, n = 3) under 30°C and 200 $\mu Em^{-2}s^{-1}$ (**Fig. 4b**). The 2% composites pretreatment reduced the final *S. elongatus* biomass concentrations by 75% compared to the BG11 control, while the same pretreatment

298 decreased final biomass concentrations of the natural algae community by 48% (**Fig. 4e, f**). Also, the
299 cyanobacteria in the pretreated medium became light green and yellowish, suggesting lower chlorophyll
300 concentrations and impaired photosynthesis (Feng et al., 2010). **Fig. 4** also shows that the low P medium
301 more severely impaired algal growth under high light intensity (e.g., a hot summer season), which is
302 consistent with a previous study (Litchman et al., 2003).

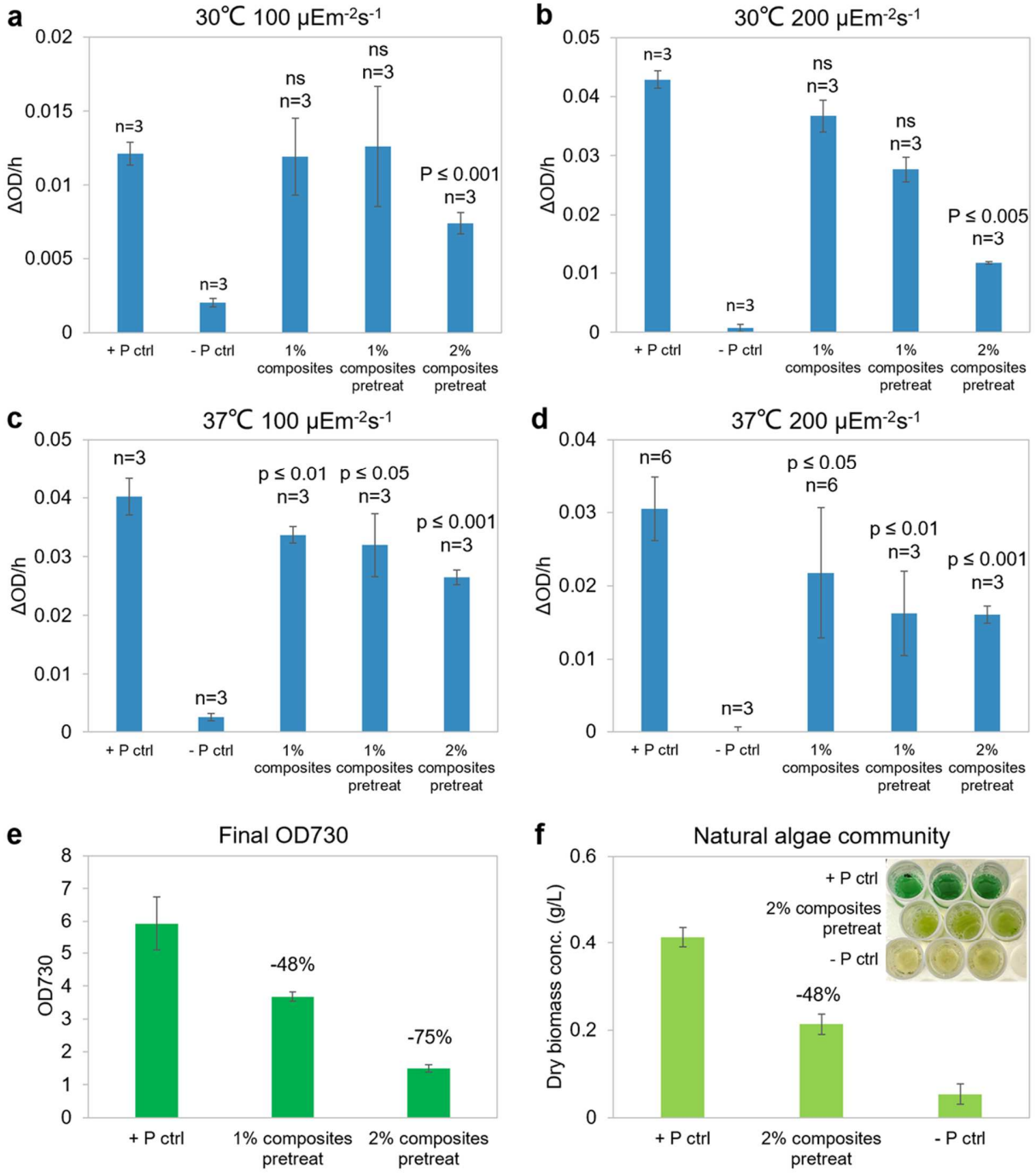

Fig. 4. Application of mineral-hydrogel composites to reduce *S. elongatus* growth. **Fig. 4a-d**: Note the differing Y axis ranges. Cell growth (OD730) change per hour at (**a**) 30℃ and 100 $\mu Em^{-2}s^{-1}$, (**b**) 30℃ and 200 $\mu Em^{-2}s^{-1}$, (**c**) 37℃ and 100 $\mu Em^{-2}s^{-1}$, and (**d**) 37℃ and 200 $\mu Em^{-2}s^{-1}$. "+ P ctrl": Normal BG11 medium; "- P ctrl": BG11 medium without P; "1% composites": culture in the presence of 1% composites; "1% or 2% composites pretreat": The BG11 medium was pretreated with either 1% (wet composites basis: 10 g/L) or 2% (wet composites basis: 20 g/L) mineral-hydrogel composites before

being used for algal culture. Conditions (initial pH, final pH) after 24 h: + P ctrl (7.46, 10.63), - P ctrl (7.62, 8.36), 2% composites pretreat (8.95, 9.38). "ns" means not significant. **Fig. 4e** and **4f** show total biomass after 7 days growth on BG11 medium treated by the mineral-hydrogel composites: (**e**) *S. elongatus* growth under 37°C and 200 $\mu Em^{-2}s^{-1}$, n=3, (**f**) natural algae community growth (including both cyanobacteria and eukaryote algae) under 37°C and 200 $\mu Em^{-2}s^{-1}$, n = 3. The final cultures were imaged for color comparison. Note that one OD_{730} is equivalent to 0.3 g/L dry biomass.

We further tested treatment of real wastewater using the mineral-hydrogel composites. As shown in **Fig. 5a**, the use of 5% w/w composites greatly reduced the dissolved P in both municipal wastewater (-96%) and agricultural run-off water (-91%). To simulate a field application of the composites, we diluted the treated water with P-free BG11 media (analogous to releasing it into a large waterbody). To keep the nitrogen concentration constant in all testing solutions, three dilution factors were used: 10x, 30x, and 100x. The controls were untreated P-rich wastewater diluted with P-free BG11 at the same rate. Then *S. elongatus* was inoculated into the diluted solutions. Compared to the control groups, both treated wastewaters showed much less algal growth (**Table 2**). For example, the algal growth reduction was -65% in treated municipal wastewater and -71% in treated agricultural run-off water (after 100x dilution).

In summary, we found that the newly developed mineral-hydrogel composites can capture P from different sources of wastewater, reducing their concentrations to as low as 0.3~0.5 mg/L. Consistent with the mineral-hydrogel composites presented in our previous works (Kim et al., 2018; Tan et al., 2021a), the mineral-hydrogel composites used here reduced P to similarly low concentration levels (0.70 mg/L in Kim et al. and 0.25 mg/L in Tan et al.), despite the interfering presence of other ions in either the BG11 medium or the complex wastewater. Such high P removal from wastewater is expected to effectively reduce eutrophication and limit HABs in aquatic systems (Carvalho et al., 2013), especially when the

temperature and sunlight are optimal for algal growth. Furthermore, the P captured by the composites is easily released in a P deficient medium over multiple cycles, resulting in 0.5–0.6 mg-P /L in the solution (**Fig. 5b**). We will investigate the composites' use as fertilizer in the next section.

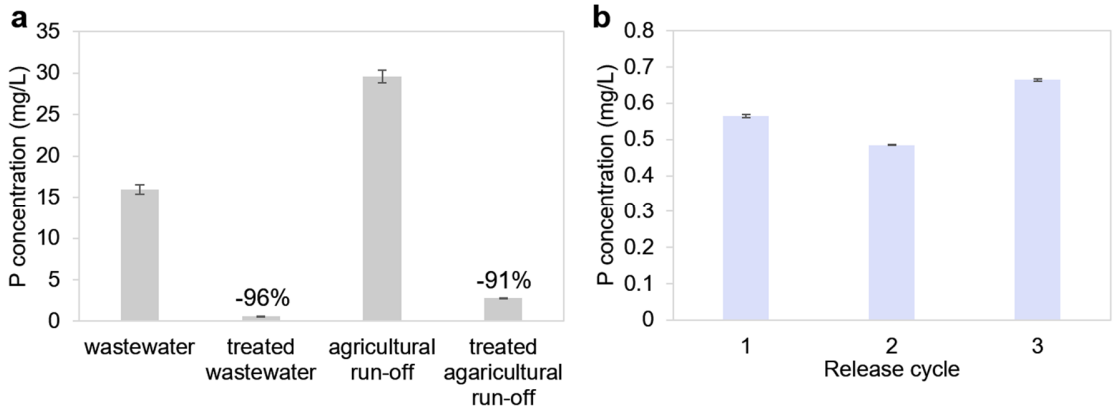

Fig. 5. Potential field applications with mineral-hydrogel composites. **(a)** 5% composites (50 g/L) treatment of municipal wastewater and synthetic agriculture run-off water. **(b)** P release from 5% P-recovered composites in three successive P-release cycles. Each P-release cycle lasted 24 hours in P-free BG11 medium, resulting in relatively constant P level in the medium.

Table 2. *S. elongatus* growth reduction% in treated wastewater and treated agricultural run-off

S. elongatus OD_{730} reduction%	Dilution factor		
	10x	30x	100x
Treated wastewater	-49 ± 1%	-59 ± 1%	-65 ± 5%
Treated agricultural run-off	-31 ± 2%	-49 ± 2%	-71 ± 5%

Note: reduction % = (1 – (OD_{730} in treated media ÷ OD_{730} in untreated media)) × 100%. Here, n = 2 and ± indicates the standard deviation.

Application of mineral-hydrogel composites to supply P for algal cultivation and lipid accumulation.

S. elongatus is a promising chassis for bioproduction (Abernathy et al., 2017). To test the recyclability (and its upcycling potential) of P-recovered composites as P nutrient delivery media, we further investigated the composites' P delivery and compatibility with cyanobacterial cultivations. Note that HAB

remediation and algal cultivation for biomanufacturing are two sides of a coin (illustrated in Fig. 1), and our mineral-hydrogel composites can operate in both contexts. In P-rich conditions, the mineral-hydrogel composites capture P from the culture medium, but under P-deficient conditions they release P through the dissolution of the mineral seed. The CaP mineral's solubility determines the switch between these two functions. In contact with algal species, the controlled release of P depends on the solution pH, calcium concentration, and algal P utilization. For example, with the calcium concentrations commonly found in municipal wastewater (20–120 mg/L) and at pH 7.5, the composites maintained 0.3–0.5 mg-P/L in the solution (**Fig 3a and 5a**). Moreover, the synergy between CaP and the wollastonite mineral seeds further improves the reusability of the composites as a P-source for photo-biorefinery applications. Compared to the results of previous studies using composites with only CaP (Kim et al., 2018; Tan et al., 2021b), the wollastonite addition increased the mineral hydrogel composites' structural integrity and resistance to mechanical stress from photobioreactor mixing (**Fig. S4**). Here, we further tested whether the slow release of P from the composites could support microalgae growth and fatty acids (biodiesel precursors) accumulations. As shown in **Fig. 6a**, the *S. elongatus* growth with fresh mineral-hydrogel composites (1%, without loading extra phosphorous) in P-free BG11 was reduced by ~50% compared to normal BG11 cultures. *S. elongatus* cultures with the same amount of composites (after P capture from synthetic wastewater) restored the growth rates by 70% in P-free BG11. As expected, severely P-limited conditions led to elongated cell sizes (**Fig. 6c**) and significantly higher fatty acid content in biomass (Peng et al., 2019; Singh et al., 2015). Compared to P-sufficient samples, *S. elongatus* cells increased their major lipid components by 3.7-fold in P-free BG11 cultures with fresh mineral-hydrogel composites, which had a

low release of P (**Fig. 6b**). In general, P-bioavailability is often used to balance lipid accumulation and biomass growth in many microalgae species, such as *Scenedesmus* sp. and *Chlamydomonas reinhardtii*. (Kamalanathan et al., 2015; Xin et al., 2010; Yang et al., 2018). In future studies, mineral-hydrogel composites can be loaded with different amounts of P to regulate algal biomass growth or lipid accumulations.

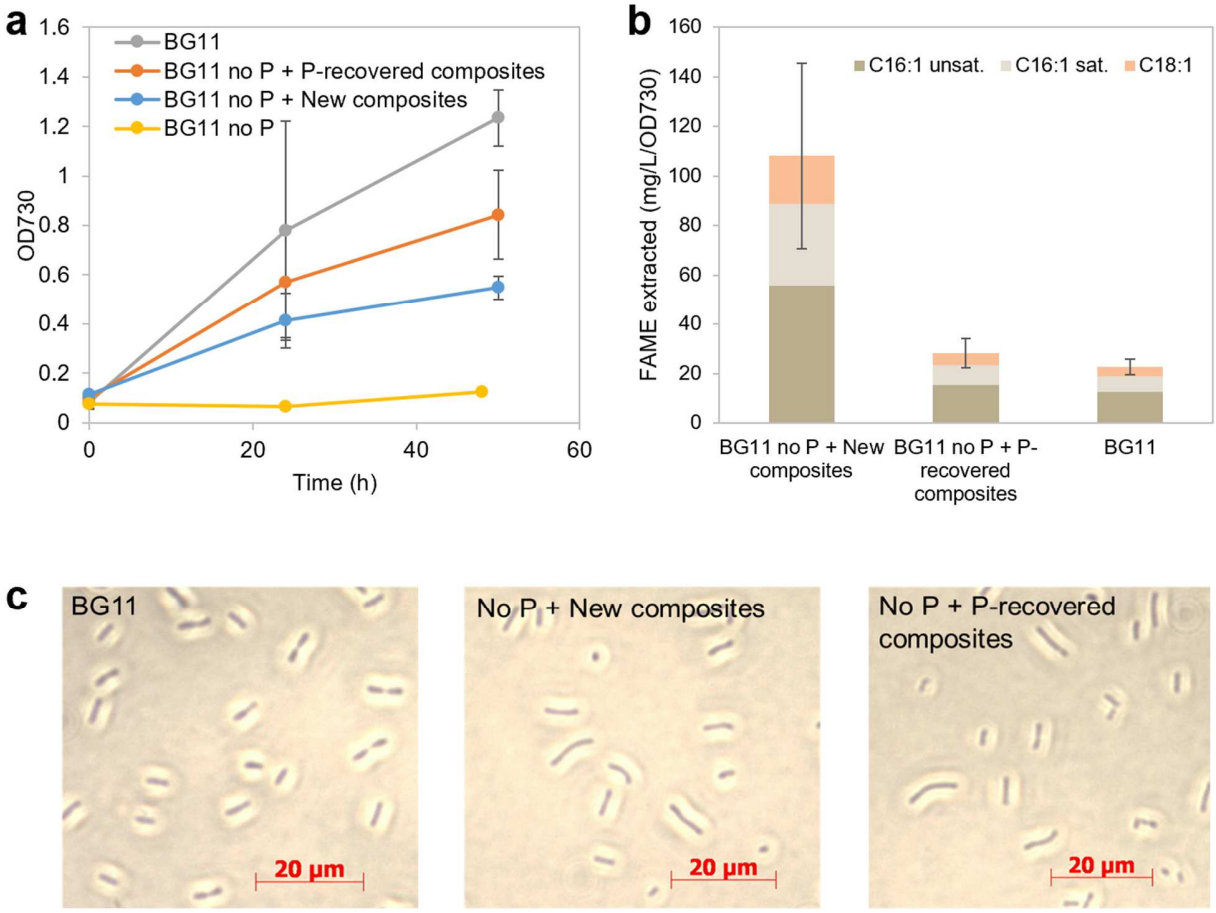

Fig. 6. The effects of P concentration on cyanobacterial growth and lipids accumulation. **(a)** Growth curves under a P-limited condition, n = 3, 1% composites (10 g/L). **(b)** Fatty acids contents in biomass (upper column segment, C14:1; middle segment, C16:1 unsaturated; bottom segment, C16:1 saturated). The fatty acid methyl esters extracted (mg FAME/L/OD730) are normalized by OD730. **(c)** Representative microscopic images of *S. elongatus* for three conditions (left, BG11; middle, no P in BG11 with new composites; right, no P in BG11 with P-recovered composites). Elongated cells indicate P-deficient stress.

384

385 **Novelty of the composites and future opportunities.** Traditional P capture methods, using chemical
386 precipitation (Marti et al., 2010; Song et al., 2006) or agents such as engineered biochar (Yao et al., 2013)
387 or activated carbon powder (Wang et al., 2018), have been proposed to remove P as well as to reuse it as
388 fertilizer (Khan et al., 2008; Ramli, 2019). Our mineral-hydrogel composites employ CaP mineral seeds
389 as a template, facilitating *in situ* heterogeneous CaP nucleation (Kim et al., 2018; Tan et al., 2021a) and
390 reducing P to low concentrations (as low as 0.3 mg-P/L). This performance has been achieved despite the
391 presence of multiple competitive and interfering cations and anions. In the tested wastewaters, the
392 composites had loadings of 5.6 and 10.6 mg-P/g-dry CaP mineral seed, exceeding loadings of many
393 reported adsorbents (**Fig. S3**) (Almasri et al., 2019; Awual, 2019; Chen et al., 2022; Cui et al., 2020; Hao
394 et al., 2019; Huang et al., 2022; Kumar et al., 2019b; Liu et al., 2019; Shan et al., 2019; Shi et al., 2019;
395 Xu et al., 2021; Zhang et al., 2021). For common adsorbents, a trade-off exists between high P-affinity
396 and the reusability of the captured P. In contrast, our mineral-hydrogel composites not only have high P
397 capture but also release P at a sufficient level to sustain algal growth. Mediated by the CaP mineral seed's
398 solubility and calcium concentrations, our composites can easily switch between P capture and release
399 modes.

400 Moreover, the added wollastonite seeds in the composites improves the reusability of the composites
401 as a P-source for photo biorefinery applications by increasing the mineral hydrogel composites' structural
402 integrity and resistance to mechanical stress (**Fig. S4**). In addition, because of their large average size
403 (~1.5 mm in diameter), the composites can be easily recovered after use. Therefore, we expect our

composites can be employed and reused by local water treatment facilities or on-site wastewater treatment systems to treat point sources of P pollution.

What's more, the P-enriched mineral-hydrogel composites do not increase water's turbidity and are made from non-toxic materials, enabling their excellent reuse as controlled P release materials for algal growth and lipid accumulations. The alginate hydrogel in the composites is also fully biodegradable at the end of its life. Compared to hydrothermal liquefaction approaches that convert algae biomass into bio-oils, followed by P recovery from the biochar (Dandamudi et al., 2021), our process not only does not generate toxic hydrothermal byproducts but also avoids the expensive catalytic process for upgrading bio-oil to biodiesel.

For large-scale application of our technology, future studies are still required. First, our mineral-hydrogel composites need to be optimized for repeated applications or reusability. Since Ca-P interaction is the dominant mechanism for P capture, multiple P capture-release cycles from composites may deplete internal Ca minerals and reduce the effectiveness of P recovery. In this case, we will have to develop convenient protocols to regenerate composites using calcium solution. Second, the composites' P capture capability is controlled by the solubility of the CaP mineral seeds (i.e., the Ca^{2+} concentration and pH of the wastewater). **Fig. S5** describes the estimated theoretical thresholds of P concentrations that can be captured by the composites as functions of Ca^{2+} and pH, based on hydroxyapatite ($Ca_5(PO_4)_3(OH)$) solubility. In municipal wastewater (calcium concentration > 20 mg/L and pH > 7), the hydrogel composites are able to reduce P below 0.3 mg/L. However, if wastewater is acidic or has low Ca^{2+} concentrations, the composites will capture less P. New methods should be developed to improve the

composites' performance in acidic and low Ca^{2+} wastewater. Third, future work is needed to investigate the cost-benefits, the life cycle, the scalability of the mineral-hydrogel composites, and their optimal application in continuous configurations.

Conclusions

Our novel mineral-hydrogel composites offer a new route for P capture that utilizes heterogeneous mineral nucleation and growth. They can reduce P to low concentrations even for complex wastewater samples. This study also shows after the composite's treatment of point source P, algal growth can be significantly reduced. After P capture, the P-recovered composites can be utilized for useful biorefinery. Specifically, the P-recovered composites can release P in a bioreactor to promote lipid accumulation by providing P for algal growth. This study presents a potential new platform that connects wastewater treatment and HAB control with sustainable bio-manufacturing. Finally, this study is a lab-scale proof-of-concept, and steps remain between this concept and its large-scale application. We hope that this work serves as a modest spur to future research on this approach to capturing phosphorus from wastewater and reusing it in biomanufacturing.

Acknowledgments

This article was developed under Assistance Agreement No. 840084, awarded by the United States Environmental Protection Agency to Professor Young-Shin Jun. It has not been formally reviewed by the EPA. The views expressed in this article are solely those of the authors and do not necessarily reflect those of the Agency. The EPA does not endorse any products or commercial services mentioned in this publication. Mr. Albern Tan acknowledges support from the National Science Foundation Graduate Research Fellowship Program (Grant #DGE-1745038). The Nano Research Facility (NRF) and Institute of Materials Science & Engineering (IMSE) at Washington University provided their facilities for the

446 experiments. Ongoing research on the application of hydrogel composites to promote large-scale algal
447 cultivation is supported by the DOE Fossil Energy Office (DE-FE0032108). We are grateful to Prof.
448 James Ballard at Washington University for careful review of our manuscript.

449 **Conflict of Interest**

450 The authors declare that they have no known competing financial interests or personal relationships that
451 could have appeared to influence the work reported in this paper.

452

References

Abernathy MH, Yu J, Ma F, Liberton M, Ungerer J, Hollinshead WD, et al. Deciphering cyanobacterial phenotypes for fast photoautotrophic growth via isotopically nonstationary metabolic flux analysis. Biotechnology for Biofuels 2017; 10: 273.

Almasri DA, Saleh NB, Atieh MA, McKay G, Ahzi S. Adsorption of phosphate on iron oxide doped halloysite nanotubes. Scientific Reports 2019; 9.

Amara S, Seghezzi N, Otani H, Diaz-Salazar C, Liu J, Eltis LD. Characterization of key triacylglycerol biosynthesis processes in rhodococci. Scientific reports 2016; 6: 1-13.

Awual MR. Efficient phosphate removal from water for controlling eutrophication using novel composite adsorbent. Journal of Cleaner Production 2019; 228: 1311-1319.

Bacelo H, Pintor AMA, Santos SCR, Boaventura RAR, Botelho CMS. Performance and prospects of different adsorbents for phosphorus uptake and recovery from water. Chemical Engineering Journal 2020; 381: 122566.

Bashar R, Gungor K, Karthikeyan KG, Barak P. Cost effectiveness of phosphorus removal processes in municipal wastewater treatment. Chemosphere 2018; 197: 280-290.

Berman-Frank I, Lundgren P, Falkowski P. Nitrogen fixation and photosynthetic oxygen evolution in cyanobacteria. Research in Microbiology 2003; 154: 157-164.

Bolton L, Joseph S, Greenway M, Donne S, Munroe P, Marjo CE. Phosphorus adsorption onto an enriched biochar substrate in constructed wetlands treating wastewater. Ecological Engineering: X 2019; 1: 100005.

Braun JCA, Borba CE, Godinho M, Perondi D, Schontag JM, Wenzel BM. Phosphorus adsorption in Fe-loaded activated carbon: Two-site monolayer equilibrium model and phenomenological kinetic description. Chemical Engineering Journal 2019; 361: 751-763.

Bujdák J. Adsorption kinetics models in clay systems. The critical analysis of pseudo-second order mechanism. Applied Clay Science 2020; 191: 105630.

Bullerjahn GS, McKay RM, Davis TW, Baker DB, Boyer GL, D'Anglada LV, et al. Global solutions to regional problems: Collecting global expertise to address the problem of harmful cyanobacterial blooms. A Lake Erie case study. Harmful Algae 2016; 54: 223-238.

Cantor B. Heterogeneous nucleation and adsorption. Philosophical Transactions of the Royal Society of London. Series A: Mathematical, Physical and Engineering Sciences 2003; 361: 409-417.

Carpenter SR, Bennett EM. Reconsideration of the planetary boundary for phosphorus. Environmental Research Letters 2011; 6: 014009.

Carvalho L, McDonald C, de Hoyos C, Mischke U, Phillips G, Borics G, et al. Sustaining recreational quality of European lakes: minimizing the health risks from algal blooms through phosphorus control. Journal of Applied Ecology 2013; 50: 315-323.

Chen D, Yu H, Pan M, Pan B. Hydrogen bonding-orientated selectivity of phosphate adsorption by imine-functionalized adsorbent. Chemical Engineering Journal 2022; 433: 133690.
Chen JJ, Thomas JJ, Taylor HFW, Jennings HM. Solubility and structure of calcium silicate hydrate. Cement and Concrete Research 2004; 34: 1499-1519.
Combes C, Rey C. Amorphous calcium phosphates: Synthesis, properties and uses in biomaterials. Acta Biomaterialia 2010; 6: 3362-3378.
Correll DL. The role of phosphorus in the eutrophication of receiving waters: A review. Journal of environmental quality 1998; 27: 261-266.
Cui QL, Xu JL, Wang W, Tan LS, Cui YX, Wang TT, et al. Phosphorus recovery by core-shell gamma-Al2O3/Fe3O4 biochar composite from aqueous phosphate solutions. Science of the Total Environment 2020; 729.
Dalahmeh SS, Stenström Y, Jebrane M, Hylander LD, Daniel G, Heinmaa I. Efficiency of iron- and calcium-impregnated biochar in adsorbing phosphate from wastewater in onsite wastewater treatment systems. Frontiers in Environmental Science 2020; 8.
Dandamudi KPR, Mathew M, Selvaratnam T, Muppaneni T, Seger M, Lammers P, et al. Recycle of nitrogen and phosphorus in hydrothermal liquefaction biochar from Galdieria sulphuraria to cultivate microalgae. Resources, Conservation and Recycling 2021; 171: 105644.
Daniel TC, Sharpley AN, Lemunyon JL. Agricultural phosphorus and eutrophication: A symposium overview. Journal of environmental quality 1998; 27: 251-257.
Davis TW, Bullerjahn GS, Tuttle T, McKay RM, Watson SB. Effects of increasing nitrogen and phosphorus concentrations on phytoplankton community growth and toxicity during Planktothrix blooms in Sandusky Bay, Lake Erie. Environmental science & technology 2015; 49: 7197-7207.
dos Santos GED, Lins PVD, Oliveira L, da Silva EO, Anastopoulos I, Erto A, et al. Layered double hydroxides/biochar composites as adsorbents for water remediation applications: recent trends and perspectives. Journal of Cleaner Production 2021; 284.
Feng X, Bandyopadhyay A, Berla B, Page L, Wu B, Pakrasi HB, et al. Mixotrophic and photoheterotrophic metabolism in Cyanothece sp. ATCC 51142 under continuous light. Microbiology 2010; 156: 2566-2574.
Gobler CJ. Climate Change and Harmful Algal Blooms: Insights and perspective. Harmful Algae 2020; 91: 101731.
Guida S, Rubertelli G, Jefferson B, Soares A. Demonstration of ion exchange technology for phosphorus removal and recovery from municipal wastewater. Chemical Engineering Journal 2021; 420: 129913.
Hao HT, Wang YL, Shi BY. NaLa(CO3)(2) hybridized with Fe3O4 for efficient phosphate removal: Synthesis and adsorption mechanistic study. Water Research 2019; 155: 1-11.
Huang Y, He Y, Zhang H, Wang H, Li W, Li Y, et al. Selective adsorption behavior and mechanism of phosphate in water by different lanthanum modified biochar. Journal of

530 Environmental Chemical Engineering 2022; 10: 107476.
531 Itodo AU, Abdulrahman FW, Hassan LG, Maigandi SA, Itodo HU. Intraparticle diffusion and
532 intraparticulate diffusivities of herbicide on derived activated carbon. Researcher 2010; 2:
533 74-86.
534 Jambor J, Dutrizac J, Groat L, Raudsepp M. Static tests of neutralization potentials of silicate
535 and aluminosilicate minerals. Environmental Geology 2002; 43: 1-17.
536 Jasinski S. Phosphate rock statistics and information: US Geological Survey, 2020.
537 Kamalanathan M, Gleadow R, Beardall J. Impacts of phosphorus availability on lipid production
538 by Chlamydomonas reinhardtii. Algal Research 2015; 12: 191-196.
539 Khan MA, Kim K-W, Mingzhi W, Lim B-K, Lee W-H, Lee J-Y. Nutrient-impregnated charcoal:
540 an environmentally friendly slow-release fertilizer. The Environmentalist 2008; 28: 231-
541 235.
542 Kim D, Wu T, Cohen M, Jeon I, Jun Y-S. Designing the crystalline structure of calcium
543 phosphate seed minerals in organic templates for sustainable phosphorus management.
544 Green Chemistry 2018; 20: 534-543.
545 Kromkamp J, van den Heuvel A, Mur LR. Phosphorus uptake and photosynthesis by phosphate-
546 limited cultures of the cyanobacterium Microcystis aeruginosa. British Phycological
547 Journal 1989; 24: 347-355.
548 Kumar PS, Korving L, van Loosdrecht MCM, Witkamp GJ. Adsorption as a technology to
549 achieve ultra-low concentrations of phosphate: Research gaps and economic analysis.
550 Water Res X 2019a; 4: 100029.
551 Kumar PS, Korving L, van Loosdrecht MCM, Witkamp GJ. Adsorption as a technology to
552 achieve ultra-low concentrations of phosphate: Research gaps and economic analysis.
553 Water Research X 2019b; 4.
554 Kumar R, Pal P. Assessing the feasibility of N and P recovery by struvite precipitation from
555 nutrient-rich wastewater: a review. Environmental Science and Pollution Research 2015;
556 22: 17453-17464.
557 Li D, Yuan Y, Cheng D, Zhao Q. Effect of light quality on growth rate, carbohydrate
558 accumulation, fatty acid profile and lutein biosynthesis of Chlorella sp. AE10.
559 Bioresource technology 2019; 291: 121783.
560 Li M, Liu J, Xu Y, Qian G. Phosphate adsorption on metal oxides and metal hydroxides: A
561 comparative review. Environmental Reviews 2016; 24: 319-332.
562 Li Y, Jin H, Liu W, Su H, Lu Y, Li J. Study on regeneration of waste powder activated carbon
563 through pyrolysis and its adsorption capacity of phosphorus. Scientific Reports 2018; 8:
564 778.
565 Lin J, Wang L. Comparison between linear and non-linear forms of pseudo-first-order and
566 pseudo-second-order adsorption kinetic models for the removal of methylene blue by
567 activated carbon. Frontiers of Environmental Science & Engineering in China 2009; 3:
568 320-324.

569 Litchman E, Steiner D, Bossard P. Photosynthetic and growth responses of three freshwater algae
570 to phosphorus limitation and daylength. Freshwater Biology 2003; 48: 2141-2148.
571 Liu RT, Chi LN, Wang XZ, Wang Y, Sui YM, Xie TT, et al. Effective and selective adsorption of
572 phosphate from aqueous solution via trivalent-metals-based amino-MIL-101 MOFs.
573 Chemical Engineering Journal 2019; 357: 159-168.
574 Mahardika D, Park H-S, Choo K-H. Ferrihydrite-impregnated granular activated carbon
575 (FH@GAC) for efficient phosphorus removal from wastewater secondary effluent.
576 Chemosphere 2018; 207: 527-533.
577 Marti N, Pastor L, Bouzas A, Ferrer J, Seco AJWr. Phosphorus recovery by struvite
578 crystallization in WWTPs: Influence of the sludge treatment line operation. 2010; 44:
579 2371-2379.
580 Mayer BK, Baker LA, Boyer TH, Drechsel P, Gifford M, Hanjra MA, et al. Total Value of
581 Phosphorus Recovery. Environmental Science & Technology 2016; 50: 6606-6620.
582 O'Neill DW, Fanning AL, Lamb WF, Steinberger JK. A good life for all within planetary
583 boundaries. Nature Sustainability 2018; 1: 88-95.
584 Paerl HW, Fulton RS, Moisander PH, Dyble JJT. Harmful freshwater algal blooms, with an
585 emphasis on cyanobacteria. 2001; 1.
586 Peng Z, Feng L, Wang X, Miao X. Adaptation of Synechococcus sp. PCC 7942 to phosphate
587 starvation by glycolipid accumulation and membrane lipid remodeling. Biochimica et
588 Biophysica Acta (BBA) - Molecular and Cell Biology of Lipids 2019; 1864: 158522.
589 Ramli RA. Slow release fertilizer hydrogels: a review. Polymer Chemistry 2019; 10: 6073-6090.
590 Reijnders L. Phosphorus resources, their depletion and conservation, a review. Resources,
591 Conservation and Recycling 2014; 93: 32-49.
592 Ritchie RJ, Trautman DA, Larkum AWD. Phosphate limited cultures of the cyanobacterium
593 Synechococcus are capable of very rapid, opportunistic uptake of phosphate. New
594 Phytologist 2001; 152: 189-201.
595 Rudzinski W, Plazinski W. Kinetics of Solute Adsorption at Solid/Solution Interfaces: A
596 Theoretical Development of the Empirical Pseudo-First and Pseudo-Second Order
597 Kinetic Rate Equations, Based on Applying the Statistical Rate Theory of Interfacial
598 Transport. The Journal of Physical Chemistry B 2006; 110: 16514-16525.
599 Schott J, Pokrovsky OS, Spalla O, Devreux F, Gloter A, Mielczarski JA. Formation, growth and
600 transformation of leached layers during silicate minerals dissolution: The example of
601 wollastonite. Geochimica et Cosmochimica Acta 2012; 98: 259-281.
602 Shan S, Tang H, Zhao Y, Wang W, Cui F. Highly porous zirconium-crosslinked graphene
603 oxide/alginate aerogel beads for enhanced phosphate removal. Chemical Engineering
604 Journal 2019; 359: 779-789.
605 Shepherd JG, Sohi SP, Heal KV. Optimising the recovery and re-use of phosphorus from
606 wastewater effluent for sustainable fertiliser development. Water Research 2016; 94: 155-
607 165.

608 Shi WM, Fu YW, Jiang W, Ye YY, Kang JX, Liu DQ, et al. Enhanced phosphate removal by
609 zeolite loaded with Mg-Al-La ternary (hydr)oxides from aqueous solutions: Performance
610 and mechanism. Chemical Engineering Journal 2019; 357: 33-44.
611 Shuler ML, Kargi F. Bioprocess Engineering: Basic Concepts: Prentice Hall, 2002.
612 Singh P, Guldhe A, Kumari S, Rawat I, Bux F. Investigation of combined effect of nitrogen,
613 phosphorus and iron on lipid productivity of microalgae Ankistrodesmus falcatus
614 KJ671624 using response surface methodology. Biochemical Engineering Journal 2015;
615 94: 22-29.
616 Solovchenko A, Khozin-Goldberg I, Selyakh I, Semenova L, Ismagulova T, Lukyanov A, et al.
617 Phosphorus starvation and luxury uptake in green microalgae revisited. Algal Research
618 2019a; 43: 101651.
619 Solovchenko AE, Ismagulova TT, Lukyanov AA, Vasilieva SG, Konyukhov IV, Pogosyan SI, et
620 al. Luxury phosphorus uptake in microalgae. Journal of Applied Phycology 2019b; 31:
621 2755-2770.
622 Song Y, Weidler PG, Berg U, Nüesch R, Donnert D. Calcite-seeded crystallization of calcium
623 phosphate for phosphorus recovery. Chemosphere 2006; 63: 236-243.
624 Tan AX, Michalski E, Ilavsky J, Jun Y-S. Engineering Calcium-Bearing Mineral/Hydrogel
625 Composites for Effective Phosphate Recovery. ACS ES&T Engineering 2021a.
626 Tan AX, Michalski E, Ilavsky J, Jun Y-S. Engineering Calcium-Bearing Mineral/Hydrogel
627 Composites for Effective Phosphate Recovery. ACS ES&T Engineering 2021b; 1: 1553-
628 1564.
629 Trapote-Barreira A, Cama J, Soler JM. Dissolution kinetics of C–S–H gel: Flow-through
630 experiments. Physics and Chemistry of the Earth, Parts A/B/C 2014; 70-71: 17-31.
631 Trottet A, George C, Drillet G, Lauro FM. Aquaculture in coastal urbanized areas: A comparative
632 review of the challenges posed by Harmful Algal Blooms. Critical Reviews in
633 Environmental Science and Technology 2021: 1-42.
634 Wang B, Gao B, Zimmerman AR, Zheng Y, Lyu H. Novel biochar-impregnated calcium alginate
635 beads with improved water holding and nutrient retention properties. Journal of
636 Environmental Management 2018; 209: 105-111.
637 Wang Z, Lee Y-Y, Scherr D, Senger RS, Li Y, He Z. Mitigating nutrient accumulation with
638 microalgal growth towards enhanced nutrient removal and biomass production in an
639 osmotic photobioreactor. Water Research 2020; 182: 116038.
640 Weissbart EJ, Rimstidt JD. Wollastonite: Incongruent dissolution and leached layer formation.
641 Geochimica et Cosmochimica Acta 2000; 64: 4007-4016.
642 Wu B, Wan J, Zhang Y, Pan B, Lo IMC. Selective Phosphate Removal from Water and
643 Wastewater using Sorption: Process Fundamentals and Removal Mechanisms.
644 Environmental Science & Technology 2020; 54: 50-66.
645 Wurtsbaugh WA, Paerl HW, Dodds WK. Nutrients, eutrophication and harmful algal blooms
646 along the freshwater to marine continuum. WIREs Water 2019; 6: e1373.

Xie Z, Walther JV. Dissolution stoichiometry and adsorption of alkali and alkaline earth elements to the acid-reacted wollastonite surface at 25°C. Geochimica et Cosmochimica Acta 1994; 58: 2587-2598.

Xin L, Hong-Ying H, Ke G, Ying-Xue S. Effects of different nitrogen and phosphorus concentrations on the growth, nutrient uptake, and lipid accumulation of a freshwater microalga Scenedesmus sp. Bioresource technology 2010; 101: 5494-5500.

Xu WS, Zheng WJ, Wang FJ, Xiong QZ, Shi XL, Kalkhajeh YK, et al. Using iron ion-loaded aminated polyacrylonitrile fiber to efficiently remove wastewater phosphate. Chemical Engineering Journal 2021; 403.

Yaakob MA, Mohamed RMSR, Al-Gheethi A, Ravishankar GA, Ambati RR. Influence of nitrogen and phosphorus on microalgal growth, biomass, lipid, and fatty acid production: an overview. Cells 2021; 10: 393.

Yang F, Xiang W, Li T, Long L. Transcriptome analysis for phosphorus starvation-induced lipid accumulation in Scenedesmus sp. Scientific reports 2018; 8: 1-11.

Yao Y, Gao B, Chen J, Yang L. Engineered Biochar Reclaiming Phosphate from Aqueous Solutions: Mechanisms and Potential Application as a Slow-Release Fertilizer. Environmental Science & Technology 2013; 47: 8700-8708.

Yu Y, You L, Liu D, Hollinshead W, Tang YJ, Zhang F. Development of Synechocystis sp. PCC 6803 as a Phototrophic Cell Factory. Marine Drugs 2013; 11.

Zarrabi M, Soori MM, Sepehr MN, Amrane A, Borji S, Ghaffari HR. Removal of phosphorus by ion-exchange resins: equilibrium, kinetic and thermodynamic studies. Environmental Engineering and Management Journal 2014; 13: 891-903.

Zehr JP. Nitrogen fixation by marine cyanobacteria. Trends in Microbiology 2011; 19: 162-173.

Zhang M, Song G, Gelardi DL, Huang L, Khan E, Mašek O, et al. Evaluating biochar and its modifications for the removal of ammonium, nitrate, and phosphate in water. Water Research 2020; 186: 116303.

Zhang Y, Akindolie MS, Tian X, Wu B, Hu Q, Jiang Z, et al. Enhanced phosphate scavenging with effective recovery by magnetic porous biochar supported La(OH)(3): Kinetics, isotherms, mechanisms and applications for water and real wastewater. Bioresource Technology 2021; 319.

Zhi Y, Zhang C, Hjorth R, Baun A, Duckworth OW, Call DF, et al. Emerging lanthanum (III)-containing materials for phosphate removal from water: A review towards future developments. Environment International 2020; 145: 106115.

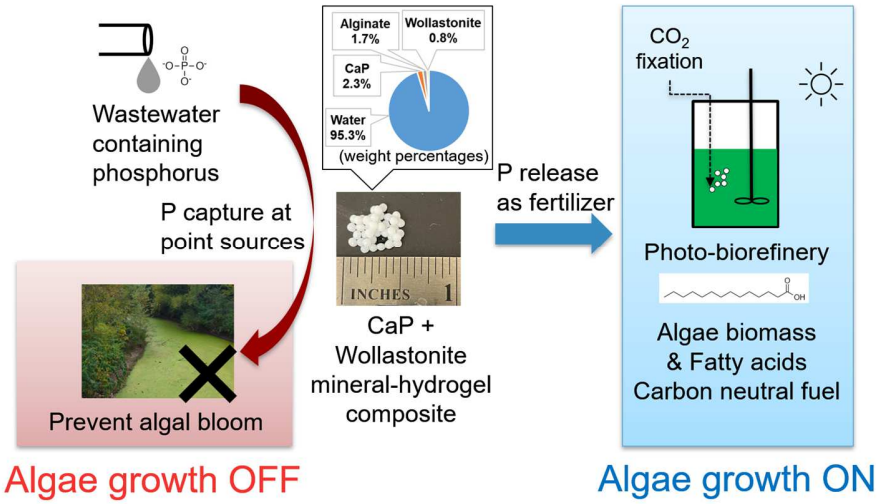
Wastewater containing phosphorus
P capture at point sources
Prevent algal bloom
Alginate 1.7%
Wollastonite 0.8%
CaP 2.3%
Water 95.3%
(weight percentages)
INCHES
CaP + Wollastonite mineral-hydrogel composite
P release as fertilizer
CO2 fixation
Photo-biorefinery
Algae biomass & Fatty acids Carbon neutral fuel
Algae growth OFF
Algae growth ON